Multiscale Phenomena of Plasma-Wall Interaction in Long Duration Discharges on TRIAM-1M

M. Sakamoto[1)], M. Ogawa[2)], H. Zushi[1)], K. Takaki[2)], M. Tokitani[2)], K. Tokunaga[3)], N. Yoshida[3)],Y. Higashizono[4)], Y. Nakashima[4)], K. Nakamura[1)], K. Hanada[1)], K.N. Sato[1)], H. Idei[1)], M. Hasegawa[1)], S. Kawasaki[1)], H. Nakashima[1)], T. Fujiwara[3)], A. Higashijima[1)], T. Shikama[5)], S. Kado[5)], A. Tsushima[6)], K. Uehara[7)], Y. Hirooka[8)], N. Nishino[9)], M. Miyamoto[10)], K. Sasaki[2)], B. Rajendraprasad[2)], M. Kitaguchi[2)], K. Nakashima[2)], Y. Nozaki[2)] and N. Kimura[2)]

1) Advanced Fusion Research Center, Research Institute for Applied Mechanics, Kyushu University, Kasuga, Fukuoka 816-8580, Japan
2) Interdisciplinary Graduate School of Engineering Sciences, Kyushu University, Fukuoka, Japan
3) Research Institute for Applied Mechanics, Kyushu University, Fukuoka, Japan
4) University of Tsukuba, Ibaraki, Japan
5) The University of Tokyo, Tokyo, Japan
6) Yokohama National University, Kanagawa, Japan
7) Japan Atomic Energy Agency, Ibaraki, Japan
8) National Institute for Fusion Science, Gifu, Japan
9) Hiroshima University, Hiroshima, Japan
10) Shimane University, Shimane, Japan

E-mail: sakamoto@triam.kyushu-u.ac.jp

Abstract. In TRIAM-1M, various phenomena of the plasma-wall interaction of long duration discharges have been investigated focusing on their length scales. The hydrogen retention in the codeposited layer which was obtained using a material probe during the long duration discharges is consistent with the global wall pumping rate estimated from the particle balance in the vacuum vessel. The global wall pumping rate in the initial phase of the discharge seems to correlate with the oxygen impurity flux, which dominates erosion and deposition on the wall and the hydrogen retention property of the codeposited layer. The codeposition and oxygen impurity play an important role in the bridge between the scales of the PWI phenomena.

1. Introduction

Issues of plasma wall interaction (PWI) are strongly related to plasma performance and stable operation. Especially for achievement of the steady state operation (SSO), those issues become more critical. PWI phenomena contain processes over a wide range of time and length scales. PWI characteristic time scales extend from ≤ ms (hydrogen diffusion in material) to order of 10's seconds (recycling variation) and order of 10^2-10^3 seconds (wall saturation) up to order of 10^6 (PFC life time). On the other hand, PWI characteristic length scales also extend from order of nm (microstructure and radiation damage) to order of μm (dust) and

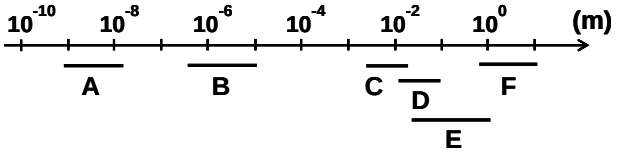

Fig.1 Characteristic length scale of PWI. A: Microstructure, Radiation damage, B: Dust, C: Hot spot, local recycling, D: Impurity transport, E: Neutral transport, F: Global particle balance

order of cm (hot spot) up to m (global particle balance) as shown in Fig.1. It is necessary to investigate comprehensively from multiscale viewpoints. In TRIAM-1M, which has capability of the SSO, the experiments of plasma-wall interaction have been carried out extensively [1-11]. In this paper, various phenomena of PWI are investigated focusing on their length scales, which are classified according to the length from the order of a diameter of the torus to that of the microstructure of the deposits on the wall. One of the key phenomena to bridge between the scales is codeposition of hydrogen with the atoms eroded from PFC.

2. Experimental Results and Discussion

One of the features of the TRIAM-1M tokamak (R_{major} ~ 0.8 m, a x b = 0.12 m x 0.18 m) is that all of the plasma facing components are made of high Z materials: the poloidal limiters (PLs) and the divertor plates are made of molybdenum, and the main chamber is made of stainless steel. A low Z material coating has never been done. A movable limiter (ML) of which front edge is made of molybdenum has been installed at the same section as the fixed poloidal limiter and the pumping port. It is thermally insulated from the main chamber and has good cooling capability. The plasma current is sustained by lower hybrid current drive (LHCD). Note that all the results reported in this paper were obtained with hydrogen discharges with a limiter configuration.

2.1 Macroscale phenomena of PWI

In order to study the multiscale phenomena of PWI, we focus on the behavior of hydrogen, molybdenum and oxygen atoms from macroscopic and microscopic viewpoints.

Firstly, the transport of neutral hydrogen in the torus and the wall recycling structure are discussed. A toroidal profile of $I_{H\alpha}$ has been measured at 6 positions in the toroidal direction as shown in Fig.2 (a). The plasma was sustained by 8.2 GHz LHCD with the power of 40kW. The line averaged electron density $\bar{n}_e$ was 0.6 x 10^{19}m^{-3}. The profile is well reproduced according to the following fitting equation;

$$I_{H\alpha}(x) = P_{mc} + \sum_{i=1}^{4} P_i \exp\left[\frac{-|x - x_i|}{\lambda}\right], \qquad (2)$$

where x is the toroidal length. P_{mc} is contribution of the main chamber recycling and is assumed to be homogeneous in the

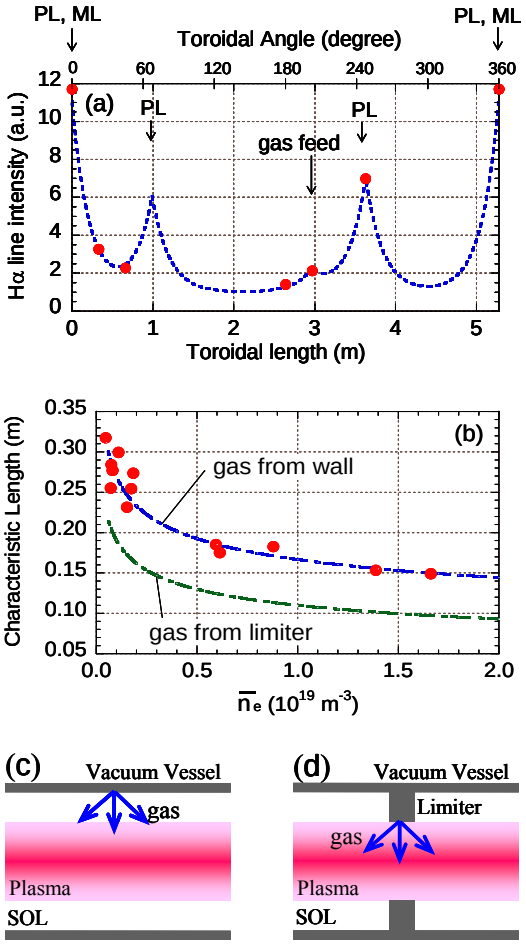

Fig.2 (a) Toroidal profile of H_α line intensity, (b) density dependence of λ estimated using equation (1). The broken lines are calculated by DEGAS simulation using cylindrical models (c) and (d).

toroidal direction. The second term of the right-hand side means the contributions of the limiters and gas fueling, respectively. The PL and the ML are strong sources of the hydrogen recycling. The recycling hydrogen neutrals travel to the toroidal direction and the hydrogen flux decays with a characteristic length λ. Figure 2(b) shows the dependence of λ on $\bar{n}_e$. The value of λ decreases not inversely but gradually with increase in $\bar{n}_e$, i.e. $\lambda \propto \bar{n}_e^{-0.2}$. The density dependence of λ can be well reproduced by DEGAS simulation [12] using a cylindrical model shown in Fig.2 (c), where a neutral source locates on the wall. By using a model shown in Fig.2 (d), where the neutral transport is blocked by the ring limiter, the data can not be reproduced. It means that the structure of $I_{H\alpha}$ profile is formed by the transport of neutrals through SOL and periphery of the plasma.

Global particle balance of the long duration discharges has been discussed using a simple particle balance equation in the main chamber as follows:

$$\frac{dN_H^0}{dt} + \frac{dN_H^p}{dt} = \Gamma_{fuel} - \Gamma_{pump} - \Gamma_{wall}, \qquad (1)$$

where N_H^0 is the total number of hydrogen neutral atoms in the chamber, N_H^p the total number of hydrogen ions in the plasma, Γ_{fuel} the fueling rate, Γ_{pump} the pumping rate by the external pump-unit and Γ_{wall} the net wall pumping rate. In the steady state condition, Γ_{wall} can simply be obtained from the balance between Γ_{fuel} and Γ_{pump}. Figure 3 shows time evolution of averaged wall pumping rate and the wall temperature of two kinds of long duration discharges. The major difference between both discharges is the wall temperature. In the discharge of Fig.3 (a), the ML was not used and the wall temperature increased partly up to 120 ^{o}C due to the heat load form the plasma. On the other hand, in the discharge of Fig.3 (b), the increase in the wall temperature was suppressed less than 60 ^{o}C by using the ML. Calorimetry revealed that 34 % of the whole heat load was dealt by the ML. The wall temperature was measured at a back side of the main chamber using thermocouples. It should be noted that the temperature distribution of the main chamber ranged from room temperature to the maximum one which is shown in Fig.3. As shown in Fig.3 (a), the averaged wall pumping rate is 2.4 x 10^{16} H m^{-2} s^{-1} in the first 30 minutes and then it transits to negative (-8 x 10^{15} H m^{-2} s^{-1}). It means that the wall plays both roles of particle sink and particle source during the discharge. It is considered that the increase in re-emission of hydrogen from the wall due to the wall temperature rise is

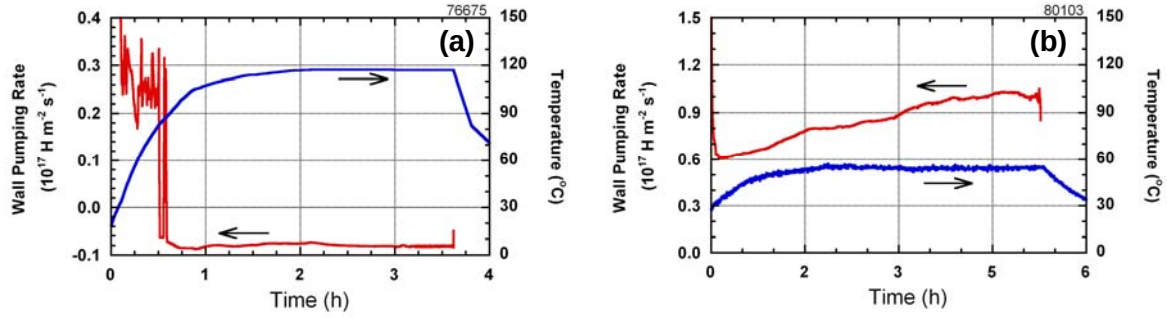

Fig.3 Time evolution of averaged wall pumping rate and wall temperature in ultra-long duration discharges with a movable limiter (a) and without one (b). The plasma density is deduced to be ~1 x 10^{18} m^{-3} for both discharges. RF power is ~7 kW and ~6 kW for the discharges of (a) and (b), respectively.

attributed to the transition of the wall role from the particle sink to source. On the other hand, when the ML is inserted to the plasma edge, the wall does not saturate until the end of the discharge (t ~ 5 h 16 min) as shown in Fig.3 (b). In this discharge, the averaged wall pumping rate is ~8.6 x 10^{16} H m^{-2} s^{-1} and it is 3.6 times higher than that of Fig.3 (a). It means that the hydrogen re-emission from the wall is suppressed due to the less temperature increase and the global wall pumping does not saturate. This continuous wall pumping would be attributed to the co-deposition of hydrogen with Mo. The detail is discussed in the next section.

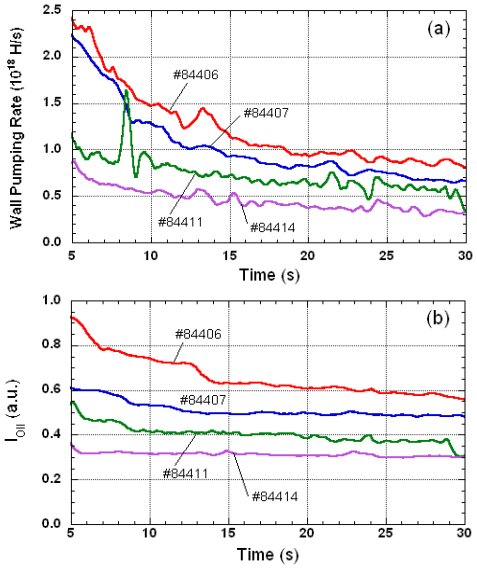

Fig.4 Time evolution of (a) wall pumping rate and OII intensity in the initial phase of the discharges.

In the previous study of hydrogen recycling [1], it is obvious that in the initial phase of the long duration discharge the hydrogen recycling coefficient increases with two time constants: a few seconds and ~30 s. In this period, the recycling coefficient changes significantly. Figure 4(a) shows time evolution of wall pumping rate in the initial phase of the long duration discharge. The decrease in the wall pumping rate means increase in the recycling coefficient. It is found that the wall pumping rate decreases shot-by-shot. The OII line intensity indicates the same tendency as the wall pumping rate as shown in Fig.4 (b). Figure 5 shows the wall pumping rate as a function of OII line intensity. The global wall pumping rate seems to correlate with oxygen behavior. As reported in reference [9], the oxygen impurity affects the physicochemical properties of the deposits and then the capability of hydrogen retention of the deposits increases significantly. The result of Fig.5 may suggest the impact of codeposition of hydrogen with oxygen and molybdenum on the global wall pumping. The detail analysis is future work.

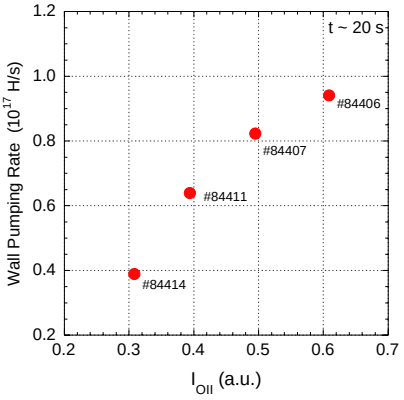

Fig.5 Wall pumping rate at t~20s as a function of the OII line intensity.

2.2 Bridge between macroscale and microscale phenomena of PWI

An in situ and real time measurement system of erosion and deposition has been developed, which is based on interference of light on a thin semi-transparent layer of redeposited material on substrate [13,14]. A sapphire window of 4mm thickness is used as a substrate, which is also used for Thomson scattering measurement. It is located at about 75 mm away from the last closed flux surface of the plasma which lies at the center of PL. A fiber optic bundle which is composed of 450 optic fibers with the diameter of 100 μm is attached to the air side

of the window. The optic fibers are mixed statistically. The fiber optic bundle is pushed on the window surface by spring action to avoid a gap between them due to vibration during the plasma production. Half of the optic fibers is used to illuminate the substrate with laser light ($\lambda \sim 635$ nm) and the other half guides the reflected light back to a photodiode. In order to avoid plasma light, an interference filter is mounted in front of the photodiode. The intensity of the laser light is monitored by the other photodiode. Figure 6 shows time evolution of the wall inventory and growth of the deposited layer in the 5-hour discharge that is shown in Fig.3 (b). The averaged growth rate of the deposited layer is ~2.3 x 10^{-4} nm s^{-1}, i.e. ~1.5 x 10^{16} Mo m^{-2} s^{-1}. The wall inventory, which is obtained from temporal integration of the wall pumping rate, is ~8 x 10^{21} H. It is found that the both of wall inventory and growth of the deposition layer indicate similar tendency. Although the spatial deposition profile on the plasma facing component is necessary for quantitative analysis, monotonic increase of the deposited layer suggests that the continuous wall pumping is attributed to the codepositoin of hydrogen with eroded Mo atoms.

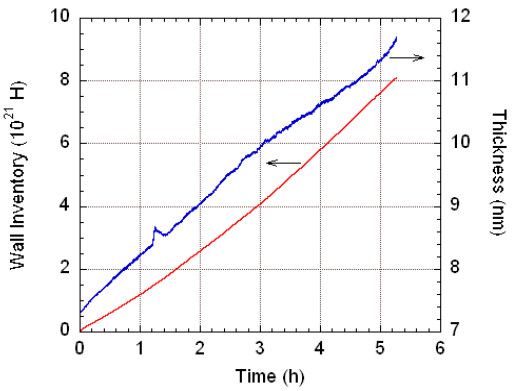

Fig.6 Time evolution of the wall inventory and growth of the deposition layer of Mo atoms sputtered on the divertor plate.

The net erosion/deposition rate on the window depends on the discharge conditions and is in the range of -2 x 10^{-3} nm s^{-1} to 2 x 10^{-3} nm s^{-1} for the long duration discharges ($0.1\text{x}10^{19}\text{m}^{-3} \le \bar{n}_e \le 1\text{x}10^{19}\text{m}^{-3}$), where plus and minus signs indicate deposition and erosion, respectively. Figure 7 shows a typical result in the high power and high density discharge. In the latter phase of the discharge, the plasma density increased due to enhanced PWI although gas fueling had been stopped. At that time, net RF power also increased, since the RF

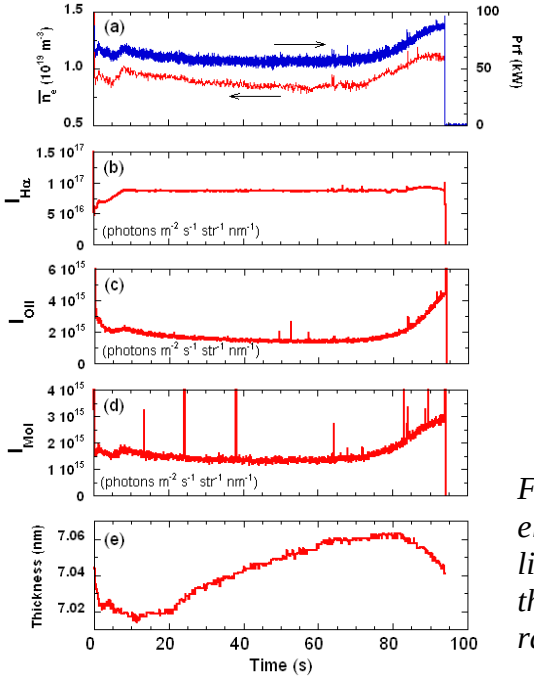

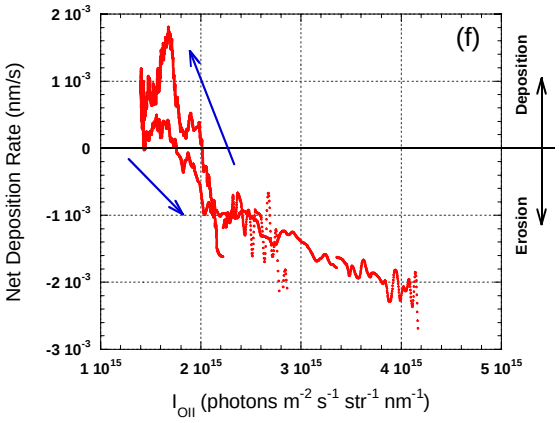

Fig.7 Time evolution of the line averaged electron density (a), H_α line intensity (b), OII line intensity (c), MoI line intensity (d), thickness of deposited layer (e), and deposition rate as a function of OII line intensity (f).

coupling with plasma was improved due to increase in SOL density and the reflected power was decreased. The OII line intensity and MoI line intensity also increased during the latter phase although H_α line intensity kept constant. It is found that the thickness of deposited layer decreased in earlier and latter phases of the discharge (i.e., erosion phase) and it increased in middle phase of the discharge (i.e., deposition phase) as shown in Fig.7 (e). Figure 7 (f) shows the deposition rate as a function of OII line intensity, which is considered to relate to oxygen flux. It seems that the oxygen impurity affects the property of erosion and there exists a critical value of oxygen flux for the transition from deposition to erosion and vice versa. In the low density discharges (i.e., low oxygen amount), the deposition rate seems to depend on a ratio of molybdenum flux Γ_{Mo} and hydrogen flux Γ_H, i.e. Γ_{Mo}/Γ_H.

2.3 Microscale phenomena of PWI

In order to study microscale phenomena of PWI, material probe experiments were carried out in the low density (~1 x 10^{18}m^{-3}) and high density (~1 x 10^{19}m^{-3}) long duration discharges [2,9,10]. The probe head with various kinds of specimens were inserted in SOL and exposed to long duration plasma and then the following analyses were carried out. The chemical composition and thickness of a deposited layer were estimated using Rutherford backscattering spectroscopy (RBS) and the concentration of hydrogen retained in the deposited layer was estimated using the elastic recoil detection (ERD). The microstructure of the deposits was observed by means of transmission electron microscopy (TEM). The results are summarized in Table 1. The major element of deposits is molybdenum. Capability of hydrogen absorption of the deposits correlates to the grain size of the deposits [9]. As reported in reference [2], the microstructure and grain size of the deposits are strongly affected by oxygen impurity. The oxygen atoms in the deposits seem to suppress free migration and crystallization of the deposited Mo atoms. The effect of oxygen on the formation of the microstructure and grain size of the deposits may correlate to the result of Fig. 5.

Table 1 Summary of results of the material probe experiments and comparison between hydrogen absorption rate Γ_{wall}^{MP} estimated by means of ERD and global wall pumping rate Γ_{wall}^{GPB} estimated using global particle balance.

	Low density (~1x10^{18} m^{-3})		High density (~1x10^{19} m^{-3})		note
	E-side	P-side	E-side	P-side	
Structure	bcc	fcc	bcc	bcc	
Grain size	10-20 nm	1-2 nm	10-20 nm	10-20 nm	
Mo depo. Rate	3.6x10^{17} Mo m^{-2} s^{-1}	6.4x10^{16} Mo m^{-2} s^{-1}	1.7x10^{18} Mo m^{-2} s^{-1}	2.3x10^{18} Mo m^{-2} s^{-1}	*x*=8mm @E-side
Γ_{wall}^{MP}	1.3x10^{16} H m^{-2} s^{-1}	6.4x10^{15} H m^{-2} s^{-1}	2.9x10^{17} H m^{-2} s^{-1}	3.5x10^{17} H m^{-2} s^{-1}	
Γ_{wall}^{GPB}	2x10^{16} H m^{-2} s^{-1} (HTW*)		4.0x10^{17} H m^{-2} s^{-1}		Whole surface area Is used. (S =5 m^2)
	8.6x10^{16} H m^{-2} s^{-1} (LTW*)				

* HTW: High Temperature Wall, LTW: Low temperature wall

3. Summary

In TRIAM-1M, PWI experiments have been carried out extensively and analyzed focusing on the behavior of hydrogen, molybdenum and oxygen atoms from the macroscopic and microscopic viewpoints. The hydrogen recycling structure does not change so much even though the plasma density changes one order of magnitude. The characteristic scale length of decay of hydrogen recycling flux in the toroidal direction depends on $\bar{n}_e^{-0.2}$. The global wall pumping rate was estimated using a global particle balance model. The wall temperature plays an important role of the hydrogen reemission of the wall. In the case of the low temperature wall, no wall saturation was observed until the ultra-long discharge with the duration of 5 h 16 min. At that time, continuous growth of the deposited layer was observed. Codeposition of hydrogen with molybdenum seems to attribute to the continuous wall pumping. In the initial phase ($t < 30$ s) of the long duration discharge, It was observed the correlation between the global wall pumping rate and the oxygen impurity flux, which may dominate erosion and deposition on the wall and the hydrogen retention property of the codeposited layer. The codeposition of hydrogen with molybdenum, and oxygen impurity flux play an important role in the bridge between the scales of the PWI phenomena.

Acknowledgement

This work has been partially performed under the framework of joint-use research in RIAM Kyushu university and the bi-directional collaboration organized by NIFS. This work is partially supported by a Grant-in-Aid for Science Research from Ministry of Education, Culture, Sports, Science and Technology.

References

[1] M. Sakamoto, et al., Nucl. Fusion **42** (2002) 165.
[2] T. Hirai et al., J. Nucl. Mater., 283-287 (2000) 1177.
[3] M. Sakamoto, et al., J. Nucl. Mater. **313-316** (2003) 519.
[4] Y. Hirooka, et al., J. Nucl. Mater. **313-316** (2003) 588.
[5] M. Sakamoto, et al., Nucl. Fusion **44** (2004) 693.
[6] H. Zushi, et al., Proc. of 31th EPS (2004) P2.129.
[7] M. Sakamoto et al., Proc. of the 32nd EPS (2005) P5.005.
[8] H. Zushi et al., Nucl. Fusion, **45** (2005) S142.
[9] M. Miyamoto et al., J. Nucl. Mater., **337-339** (2005) 436.
[10] M. Tokitani et al, Proc. of 12th ICFRM (2005) (to be published in J. Nucl. Mater.)
[11] K. Hanada et al., Fus. Eng. Design **81** (2006) 2257.
[12] D. Heifetz, D. Post, M. Petravic *et al.*, J. Comput. Phys. **46** (1982) 309.
[13] F. Weschenfelder, P. Wienhold and J. Winter, J. Nucl. Mater., **196-198** (1992) 1101.
[14] M. Sakamoto et al., Proc. of 17th PSI (2006) P1-26.